Available online at www.sciencedirect.com
ScienceDirect
Cement and Concrete Research 38 (2008) 522–529
Cement and Concrete Research

The microstructure of dispersed and non-dispersed fresh cement pastes — New insight by cryo-microscopy

Anatol Zingg [a,*], Lorenz Holzer [a], Andres Kaech [b], Frank Winnefeld [a], Joachim Pakusch [c], Stefan Becker [c], Ludwig Gauckler [d]

[a] Empa, Swiss Federal Laboratories for Materials Testing and Research, Laboratory for Concrete/Construction Chemistry, Ueberlandstrasse 129, 8600 Duebendorf, Switzerland
[b] ETH, Swiss Federal Institute of Technology Zurich, Electron Microscopy Centre Zurich (EMEZ), Schafmattstrasse 18, Zurich, Switzerland
[c] BASF AG, GKD/C-B1, Carl-Bosch-Strasse 38, 67056 Ludwigshafen, Germany
[d] ETH, Swiss Federal Institute of Technology Zurich, Institute of Nonmetallic Inorganic Materials, Department Materials, Wolfgang-Pauli-Strasse 10, 8093 Zurich, Switzerland

Received 25 May 2007; accepted 20 November 2007

Abstract

This study aims to give new insights to the microstructural development of fresh cement pastes without and with polycarboxylate-type (PCE) of superplasticizers. Qualitative comparisons of the particulate structure of such cementitious systems were carried out by using cryo-FIB and cryo-SEM techniques. The natural structure of fresh cement pastes was preserved by high pressure freezing.

It is illustrated that non-dispersed cement systems tend to form hydration rims on the surface of the clinker grains immediately after mixing. This leads to an interlocking of the particles. In contrast, in the dispersed systems the early hydrates precipitate in the pore solution and thus, agglomeration is prevented. These microstructural observations are important aspects of the fluidization effect of superplasticizers.

Keywords: Microstructure; Cryo-SEM; Cryo-FIB; Superplasticizer; Cement paste

1. Introduction

In order to enhance the workability of cements, mortars and concrete, superplasticizers are widely used. It is assumed, that the molecules of the superplasticizers adsorb onto particles surfaces and evoke mainly electrostatic (e.g. polynaphthalin-sulphonate type of superplasticizers) or electrostatic and steric (polycarboxylic-ether type of superplasticizers) repulsive forces [1–4]. As shown in Fig. 1, the addition of superplasticizers has two main rheological effects: fluidization and retardation. The viscosity is decreased due to electrostatic and steric stabilization of the cement paste [5–8]. In addition to this fluidization effect, superplasticizers also often interfere with the hydration process, which usually leads to a retardation of the setting (stiffening of the material).

These superplasticizer-effects depend on numerous parameters such as chemical composition of cement and pore solution, type of hydrate-phases, particle size distribution and water-to-cement ratio. It is assumed that these parameters also have a strong influence on the microstructure of the fresh cement paste. As illustrated schematically in Fig. 2, the addition of superplasticizers can influence the microstructure of hydrating cement systems on different scale levels: presence of polymers can strongly affect shape and size of nuclei and growing hydrates. The latter is usually far below the μm-scale. Also the spatial distribution of hydrates can be affected by addition of superplasticizers. Agglomeration process can take place at smaller and at larger scales, whereby clinker particles and hydrates start to flocculate. Close to the setting time, these particle interactions may lead to the formation of long range particle network structures. The

* Corresponding author.
E-mail address: azingg@postmail.ch (A. Zingg).

0008-8846/$ - see front matter © 2007 Elsevier Ltd. All rights reserved.
doi:10.1016/j.cemconres.2007.11.007

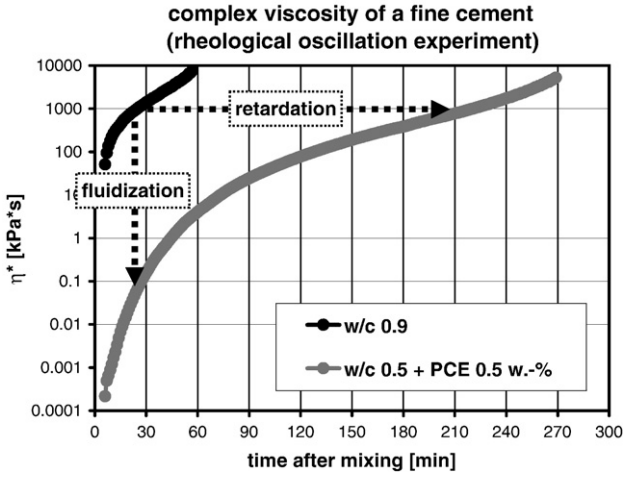

Fig. 1. Temporal evolution of the complex viscosity (obtained by rheological oscillation experiments) of fresh cement pastes (fine fraction of OPC, d_{50}=5 μm) without and with PCE. The figure illustrates the effects of fluidization and retardation [7,8] due to the addition of PCE.

understanding of the microstructural processes is still limited due to a lack of suitable microscopic methods. New methods for the microstructural investigation of fresh cement pastes have to be developed in order to improve the understanding of the effects of superplasticizers.

Most microstructural investigations on fresh cement pastes have been carried out on filter residues after removal of the pore solution. BSE-imaging with ESEM and SEM is well suited for morphological studies and size measurements of individual particles [9–15] or for microstructural characterization of hardened cement pastes. However, by applying conventional SEM sample preparation techniques the original particle arrangements of fresh cement pastes are destroyed by removing the pore solution. Investigations on filter residues for instance, should take into account that fine particles which were originally floating in the pore solution are deposited in a compacted sediment. Therefore, microstructural investigations on hydration rims and particle deposition of filter residues and polished epoxy-fixed samples should be treated with caution. The original particle arrangements of bulky hydrated, fresh cement pastes can only be preserved by high pressure freezing [16–18]. Under high pressure condition (2 kbar) the melting point for ice is shifted to −20 °C which gives the benefit of increased viscosity and decreased diffusion rates. As a consequence, homogeneous nucleation of ice is favoured whereas the mobility of ice nuclei is decreased. This prevents formation of artefacts. In contrast, conventional freezing techniques such as plunge freezing may lead to severe ice crystal damage by fast growing, large ice crystals in specimens thicker than 10 μm and hence to an artificial rearrangement of the microstructure [19–22]. High pressure freezing is essential for the preservation of the ultra-structure of soft condensed and hydrated matter. This technique was developed and well established in life sciences [23–26].

Recently, high pressure freezing has been combined with FIB-nt (Focused-Ion-Beam Nanotomography) [27,28]. Cryo-FIB-nt is based on a serial sectioning procedure using a dual-beam FIB. From each section, a BSE image is taken with the electron beam. The dimensions of such data volumes commonly measure around 20×20×20 μm and each section has a thickness of 40 nm. For the first time, a tomography method enables high resolution 3D-analysis of particles in fresh cement pastes whereby even small nuclei in the 100 nm range can be identified reliably. This opens new possibilities for quantification of particle size distribution and corresponding surface area

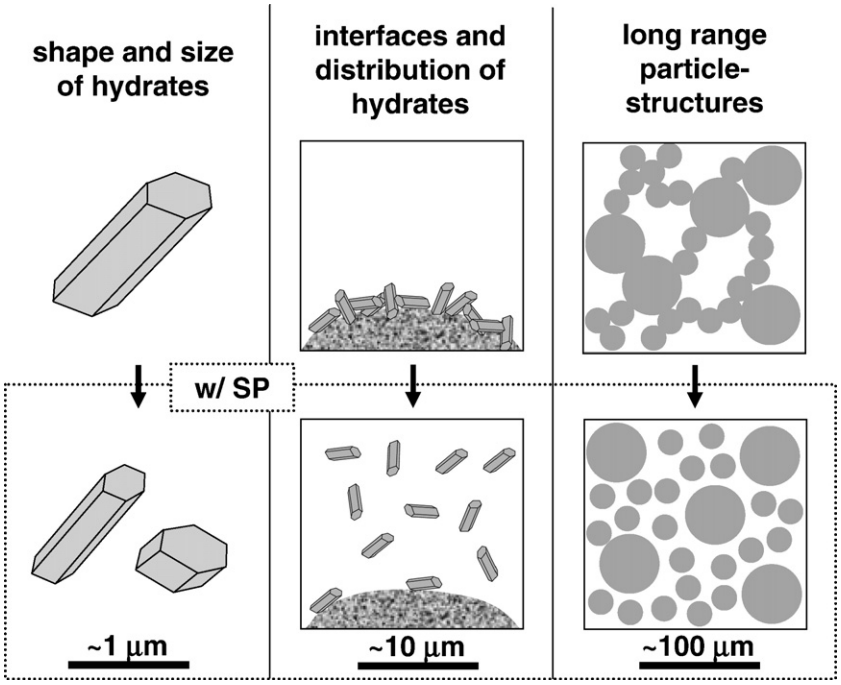

Fig. 2. Schematic illustration of the three major microstructural effects due to addition of PCE: i) change of shape and size of hydrates, ii) change of interfaces and distribution of hydrates and iii) change of the long range particle structures.

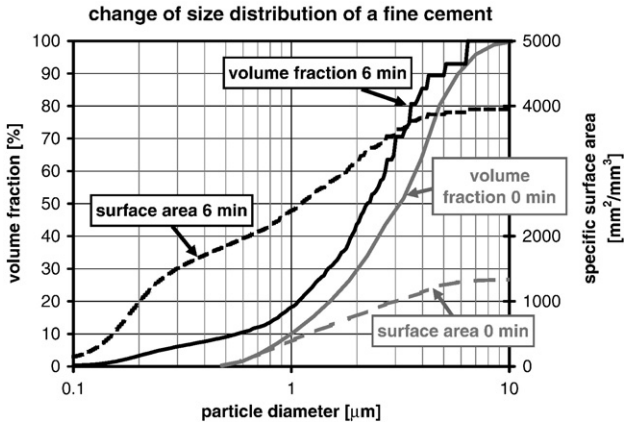

Fig. 3. Particle size distribution of a fresh paste with a fine cement was measured after 6 min of hydration with cryo-FIB-nt (figure modified after Holzer et al. [29]). The comparison with the same sample in the unhydrated state illustrates a strong increase of particles at the submicron-scale within the first 6 min. These early precipitations also lead to an increase of the specific surface area (see Section 2 for description of paste mixtures: unhydrated/0 min = sample 1, hydrated/6 min/PCE = sample 3).

in fresh cement pastes as described by Holzer [29]. The particle size distribution shown in Fig. 3 illustrates a remarkable shift to smaller grain sizes within the first few minutes of hydration due to nucleation and precipitation of hydrates (10% of the solids volume smaller than 500 nm). Simultaneously the formation of small crystals leads to an increase of the specific surface area by a factor of three.

The gain of 3D-data by serial sectioning with cryo-FIB-nt is very time consuming and this puts strong limitations to the application of this 3D-technique for extended investigations of the cementitious multi-parameter system. In addition, the data processing of such huge image stacks requires considerable computing power. The computing time for the extraction of parameters like particle size distribution, number of particles, surface area and possible particle contacts is in the range of several days. However, for quantitative characterization of 3D structures, this procedure is inevitable. Instead of excavating a cube with the ion beam and subsequent serial sectioning for 3D analysis, only a vertical cross-section can be cut into the sample. The performance of single cryo-FIB cross-sections as a shortened procedure is less time consuming and, on a qualitative level, this 2D-technique gives comparable insight to the particle structure of fresh cement pastes. Nevertheless, the magnification of cryo-FIB cross-sectioning is limited to a voxel resolution of approximately 20–40 nm mainly due to charging-problems. For more detailed investigations of fine structures at very high resolution, cryo-SEM (pixel resolution 2–4 nm) is a powerful tool which gives complementary information to cryo-FIB(nt). The data is acquired from fractured surfaces of high pressure frozen samples. High resolution cryo-SEM enables to investigate detailed surface morphologies, grain textures of hydrate layers, structural interfaces between particles and shape and size of precipitates far below 100 nm.

In this paper, cryo-FIB and cryo-SEM are used to visualize the difference of a non-dispersed and a well dispersed cement–water system for the first time. The investigations concentrate on qualitative descriptions of early hydration products, their spatial distribution, interfaces and surface morphologies. This microstructural information gives new insight into the principle mechanisms of superplasticizers.

2. Materials and methods

FIB cross-sections are limited to an approximate image-size of 50 × 50 µm due to the time consuming erosion procedure. In order to obtain statistically reasonable results (i.e. analysis of a representative volume), fine grained Portland cements with a high specific surface area (prepared by grinding or by air separation) have been used.

2.1. Raw materials

Cement I is a fine fraction of a CEM I 42.5 N, air separated, with d_{10} = 1.0 µm, d_{50} = 3.2 µm and d_{90} = 5.8 µm. Due to the separation method, cement I is enriched with alkaline-sulphates, gypsum and calcite as indicated by chemical analysis in Table 1.

Cement II is also a sample of a CEM I 42.5 N (same as for cement I), which was ground with a laboratory disc mill (Siebtechnik GmbH, Germany), with d_{10} = 0.6 µm, d_{50} = 9.0 µm and d_{90} = 37.6 µm. In order to avoid undersulfatisation, gypsum was added to a total of 4 wt.% SO_3 (Table 1).

In this study, a superplasticizer based on anionic, comb-shaped polycarboxylic-ethers (hereinafter called PCE) with low density of short, grafted polyethylene-oxide (PEO) units with methyl (Me) end groups has been used. This PCE has a molecular weight of 19,000 g/mol. It is characterized by strong adsorption and retardation behaviour on both cement types (unpublished results).

2.2. Samples

The following cement pastes were investigated with cryo-microscopy:

1. Unhydrated cement I, dispersed in a glycolic matrix, with a glycol/cement weight ratio of 0.55 which is equivalent to a volumetric proportion of a water/cement weight ratio of 0.5
2. Cement I, w/c = 0.50, hydrated for 24 min
3. Cement I, w/c = 0.50, PCE addition of 0.2 wt.% of cement I, hydrated for 6 min
4. Cement II, w/c = 0.55, PCE addition of 0.7 wt.% of cement II, hydrated for 6 min

Table 1
Chemical composition of the fine cements used

	CaO	MgO	SiO_2	Al_2O_3	Fe_2O_3	Na_2O	K_2O	SO_3	CO_2
	wt.%	wt.%	wt.%	wt.%	wt.%	wt.%	wt.%	wt.%	wt.%
Cement I (air separated)	58.0	1.6	15.8	4.2	2.2	0.2	2.1	7.3	6.8
Cement II (disc mill)	63.4	1.8	20.0	4.8	2.5	0.1	0.9	4	1.9

2.3. Methods

2.3.1. High pressure freezing

For this study, high pressure freezing was performed with a HPM 010 apparatus (BAL-TEC AG, Balzers, Liechtenstein). Kinetic and thermodynamic aspects of high pressure freezing and associated vitrification of water are discussed extensively in Bachmann [25] and Moor [26]. The complete preparation process from "paste" into the "cryo-SEM/FIB chamber" can be schematically followed in Fig. 4. Because of the high alkalinity of the cement pastes (pH >13), inert brass specimen carriers (TedPella Inc.) were used. A droplet of a cement paste was mounted on a "bottom" planchet (type A) with a cylindrical cavity depth of 100 μm and then covered with a flat "top" planchet (type B). The brass sandwich was then high pressure frozen with pressurized, supercritical nitrogen at 2100 bar.

Note that different PCE-architecture, PCE-concentrations and different hydration times result in different freezing behaviour and morphology of the pore solution. Therefore, fracturing, etching (sublimation of water), coating and imaging techniques vary strongly, depending on the sample and microscopy technique. The different sample treatments are described in the following subchapters (cryo-SEM and cryo-FIB cross-sections).

2.3.2. Cryo-SEM

In a liquid nitrogen bath, the high pressure frozen specimen carrier sandwich was vertically mounted on a cold specimen holder (Bal-Tec). The sandwich was then notched with a cooled saw blade. Afterwards the top planchet was pushed off and the specimen holder was transferred onto the cold stage of a freeze-fracturing/etching/coating device BAF060 (Bal-tec).

Subsequently, the sample was fractured by bending the sample planchet with the BAF microtome. The fractured surface was etched at −105 °C for 5 min. By using electron beam evaporation, the revealed surface was coated with 2 nm of Pt/C at an angle of 45° (~65 mA) and with an additional 1 nm of Pt/C by moving the gun between an angle of 45° and 90°. The specimen was then transferred onto the cold stage (−115 °C to −120 °C, vacuum $2.5*10^{-7}$ mbar) of a LEO Gemini 1530 SEM. All transfers were performed using the high vacuum cryo-transfer system VCT 100 (Bal-tec) [30,31].

2.3.3. Cryo-FIB cross-sections

The cryo-FIB cross-sections were obtained with a dual-beam FIB–SEM microscope (FEI Strata DB 235). The cryo-extensions and accessory units are similar to those described for cryo-SEM.

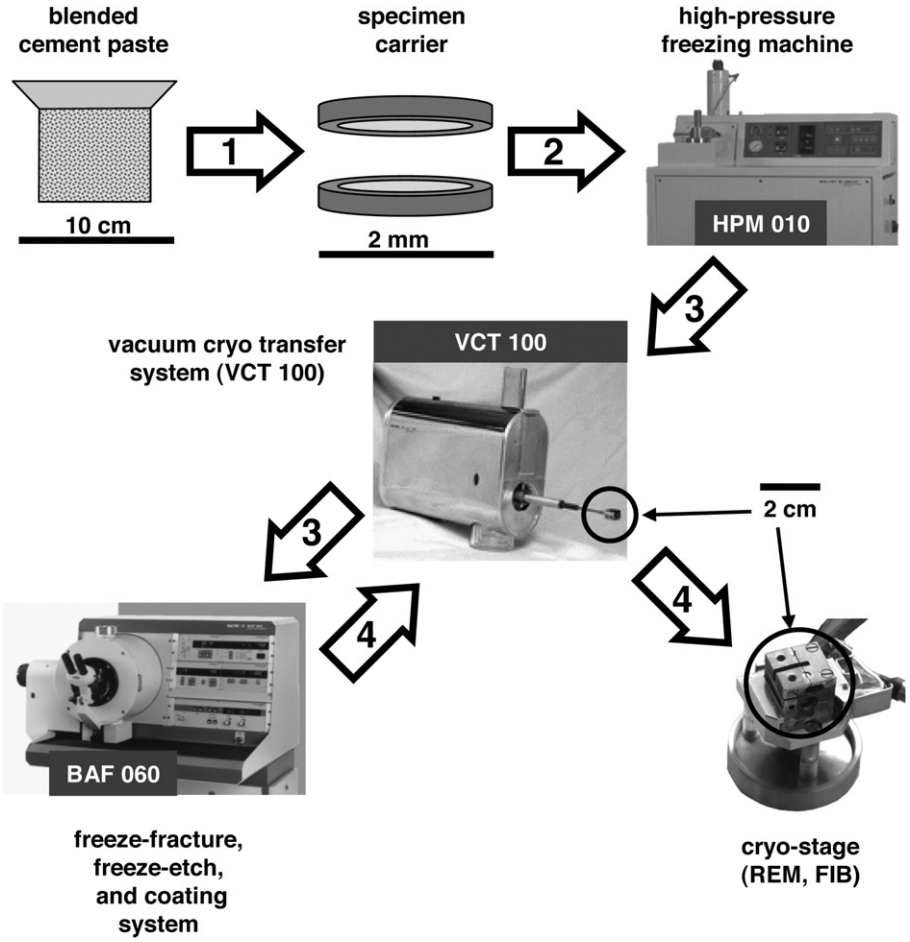

Fig. 4. Cryo-sample preparation. 1) Blended cement paste is mounted on a brass specimen carrier, 2) specimen carrier sandwich is placed in the high pressure freezing machine HPM 010, 3) transfer of frozen sample for fracturing, etching and coating in a BAF 060 and 4) transfer of the sample on the cryo-stage in the cryo-SEM chamber.

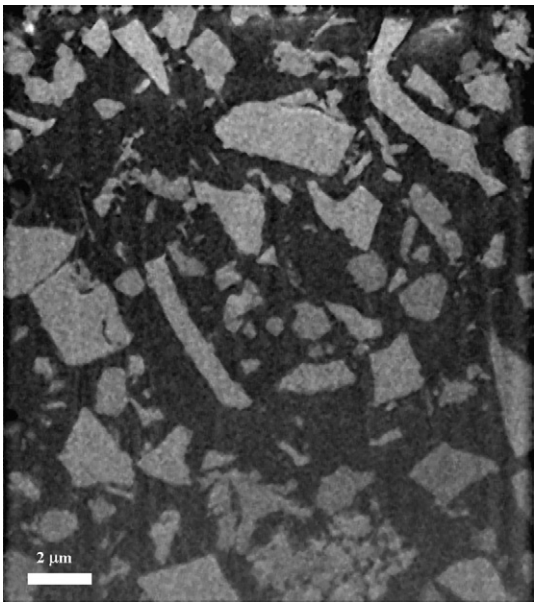

Fig. 5. Cryo-FIB cross-section (image width: 18 μm) of the unhydrated sample 1: fine fraction of an OPC (cement I), embedded in frozen glycol-matrix, volumetric proportions equivalent to w/c ~0.50. The sample has been high pressure frozen and coated with Pt.

The fractured samples were sputtered with Pt in a MED 020 (Bal-Tec) for several minutes at 65 mA. After transfer to the FIB, a metallorganic layer of several hundreds of nanometre thickness was deposited on the surface of the fractured sample. Subsequently vertical cuts with cross-sectional areas of around 10 μm × 20 μm have been eroded with the ion beam. After erosion, backscattered electron images were taken from these cross-sections. In order to avoid charging low beam voltage (3 kV), spot size (2) and relatively fast scan times (30 s) have been used.

Fig. 6. Cryo-FIB cross-section (image width: 18 μm) of a non-dispersed, strong agglomerating cement paste (sample 2, hydrated for 24 min): the paste has been high pressure frozen and coated. Note the numerous small particles (<1 μm) which are not present in the unhydrated sample (Fig. 5).

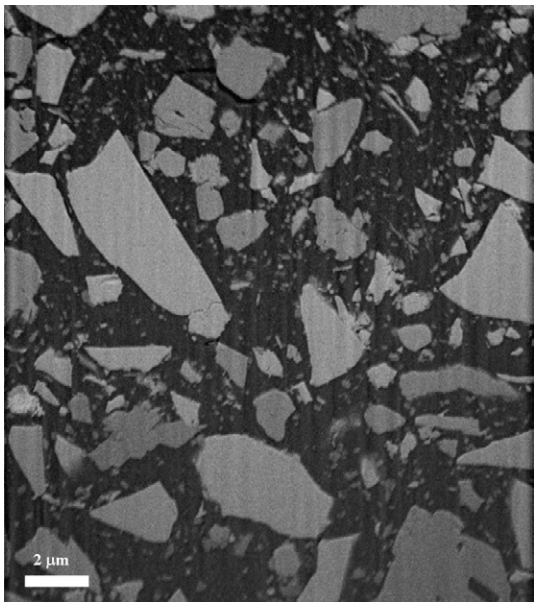

Fig. 7. Cryo-FIB cross-section (image width: 18 μm) of dispersed sample 3: fine fraction of OPC with PCE hydrated for 6 min. Note that the population of fine particles (<0.5 μm) is well dispersed in the interstitial pore space.

3. Results

Cryo-FIB enables the investigation of well-defined cross-sections, because the exposed microstructure is not biased by selective fracturing along zones of weaknesses. Hence, cryo-FIB delivers a more representative microstructural insight compared to high resolution cryo-SEM or ESEM investigations. Cryo-FIB cross-sections can be a basis for estimations of volume fractions from different grain-populations. In Figs. 5–7 the spatial distribution of large unhydrated clinker particles and small hydration phases are demonstrated for three different samples: an unhydrated, a non-dispersed (without PCE) and a well dispersed (with PCE) cement paste. Figs. 5 and 6 are taken from two 3D-FIB-nt stacks. The curves in Fig. 3 are calculated from those two stacks. Complementary to cryo-FIB, high resolution cryo-SEM allows insights to fine structures of surfaces, hydration rims and interfaces between fractured clinker particles and pore solution. Figs. 8 and 9 illustrate the high degree of microstructural details that can be resolved with this technique.

It has to be mentioned that the two systems compared in Figs. 6 and 7 are characterized by different reaction kinetics. The setting times are 140 min for sample 2 (Fig. 6) and 400 min for sample 3 containing PCE (Fig. 7). However, it was observed in our investigations that the microstructures of both systems are hardly changing during the first hours of hydration after the initial reactions of the initial period (<5 min).

Fig. 5 shows the particle structure of sample 1 (cement I dispersed in a glycolic matrix), which represents the microstructure of the unhydrated cement paste at hydration time 0. The particles of the unhydrated cement are irregularly shaped,

but they show clean and sharp boundaries. The glycolic matrix seems to be free of very fine particles. As shown in Fig. 3 the particle size distribution determined from 3D-data volume (cryo-FIB-nt) of the unhydrated cement is quite broad, ranging from several microns down to the submicron-scale. However, the volume fraction of particles at the submicron-scale is less than 10% and the fraction smaller than 500 nm is close to 0%.

In the non-dispersed cement paste (hydrated for 24 min), two populations of particles can be distinguished (Fig. 6) based on size, shape and grey-scale: the population with larger particles (size of 2–5 μm) consists of mostly bright-grey, polygonal shaped grains. These are interpreted as mostly unhydrated clinker grains. The population with the smaller particles (<500 nm) appears in a slightly darker grey level and can be interpreted as hydration products. Note, that these small particles are not present in the unhydrated sample (Fig. 5). The small particles are not dispersed in the interstitial space (as in Fig. 7) but they are attached to the surface of the unhydrated clinker particles. The density of attached particles varies. Locally they can form very dense layers, where single particles can hardly be distinguished. In other places they form very loose formations, where individual prismatic particles can be identified. The larger clinker particles either show clean boundaries or a dark, irregularly shaped rim whereas the large clinker particles are randomly distributed and the small particles at (sub-) μm-range are flocculated. Thus, agglomerates consisting of the smaller particles form bridges between the neighbouring clinker particles. The size of the agglomerates is typically between 1 and 3 μm.

In well dispersed cement pastes (Fig. 7, 6 min) the interstitial pore space between the larger clinker particles contains well dispersed crystals that are typically smaller than 500 nm. Those small crystals are very numerous and almost evenly sized. In contrast to the non-dispersed system (compare Fig. 6), the clinker particles in the dispersed system show clean boundaries, almost without any hydration rims. Only few small particles are attached to the boundaries of the larger particles. Since the small particles do not form agglomerates, the flocculation of the larger particles has not yet started. The small particles in the interstitial pore space correspond to the fraction of submicron particles as shown in Fig. 3. Up to 10% of the total solids volume is represented by particles smaller than 500 nm, which are not present in the unhydrated cement sample. The small particles in the interstitial pore space are interpreted as fresh precipitates that have formed within the first 6 min (compare Fig. 5).

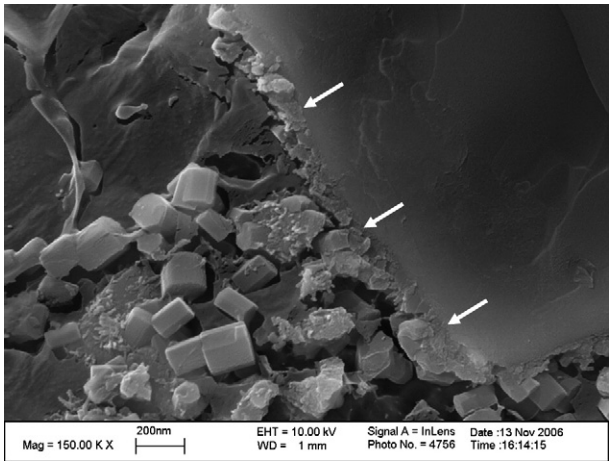

Fig. 8. High resolution cryo-SEM image of sample 4 (dispersed and hydrated for 6 min), showing ettringite (left) dispersed in pore solution and a thin, but dense hydration rim (white arrows) on the surface of a fractured, unhydrated clinker grain (right).

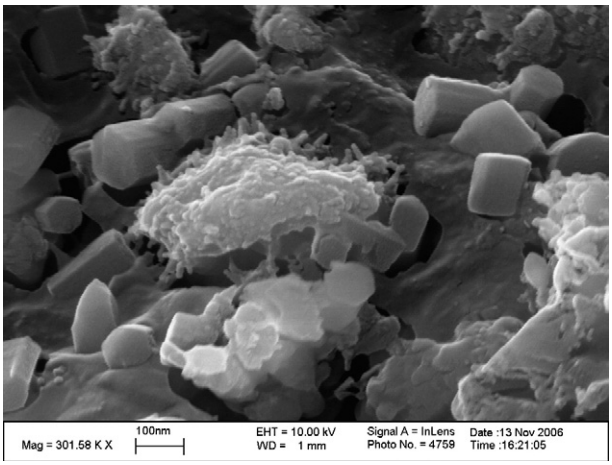

Fig. 9. High resolution cryo-SEM image of sample 4 (hydrated for 6 min) showing small fibrous hydration products which are covering hexagonal ettringite. Note that in this system with a high concentration of PCE (0.7%), most of the ettringite is well dispersed within the interstitial pore space.

Based on high resolution cryo-SEM important morphological details can be observed which are relevant for the interpretation of the smaller particle population that was previously described as hydration products based on cryo-FIB cross-sections (Fig. 7). This additional information is illustrated for the dispersed system, hydrated for 6 min, in Figs. 8 and 9.

Besides the large, fractured clinker particle in the top right corner, two different types of hydration products can be distinguished in Fig. 8. The euhedral crystals are hexagonal and short-prismatic and typically have a length of 100 to 500 nm. The thickness of these crystals is variable. Based on their morphology, these crystals can be identified as ettringite. The second population of hydration products consists of finer and fibrous minerals (possibly C–S–H) that are agglomerated and partially intergrown with ettringite crystals. As indicated in Fig. 8 with arrows, both euhedral ettringite and the fine fibres are forming together a dense rim of hydration products on the surface of the clinker particle. This rim varies in thickness between almost 0 to 200 nm.

At higher magnification (Fig. 9) it can be observed, that the smaller, fibrous crystals are covering an assemblage with numerous larger ettringite crystals. The small fibrous crystals have a thickness of 20–40 nm and they are randomly oriented and distributed on the surface of the larger ettringite.

4. Discussion

Once the initial hydration peak (after around 5 min) is over, no significant changes in the particle structures could be observed

within the first hour of hydration (dormant phase). This circumstance could be observed throughout all cryo-investigations and thus, allows qualitative comparison of samples with slightly different hydration times within the early stage of the dormant phase (5–30 min).

The unhydrated cement I contains a low percentage of the particle size fraction below 1 μm (Fig. 3). The clinker particles show relatively clean surfaces (Fig. 5). During the initial hydration phase, nucleation and precipitation of numerous small crystals (mainly ettringite) take place which results in an increase of the specific surface area. These initial hydration reactions can be observed in both, non-dispersed and dispersed cement pastes. The cryo-methods presented in this study, for the first time enable a direct comparison of the microstructures of fresh cement pastes with and without PCE. According to Fig. 3, in a fresh cement paste with PCE, the size fraction of particles in the submicron range and the corresponding specific surface area increase significantly during the first 6 min. The corresponding cryo-FIB cross-section (Fig. 7) shows that the hydrate crystals (mainly ettringites) are well dispersed in the interstitial pore space. This can be attributed to electrostatic and steric repulsive forces evoked by the adsorption of PCE molecules on the surfaces of clinker and hydrate particles. Those forces hinder the particles from precipitating onto clinker surfaces and prevent the system from agglomeration. Nevertheless, at high resolutions, cryo-SEM images of high pressure frozen fresh cement pastes with PCE locally also show fine hydration rims (Fig. 8). Some minor agglomerates of ettringite in the range of few hundreds of nm in diameter can be observed (Fig. 9). The surfaces of these agglomerates are covered with a very thin layer of small fibrous crystals that are embedded in a gel-like mass and result in an increase of surface roughness. The chemical nature of these fibrous crystals and the gel can not be analysed by the microscopic methods used but can be interpreted as very early C–S–H phases. However, in contrast to the numerous ettringite precipitates (100–500 nm) the small C–S–H needles (<50 nm) do not form individual particles. With quantitative microscopic methods (cryo-FIB-nt) only particles larger than 50–100 nm can be measured. The surface roughness of C–S–H is below this resolution and hence C–S–H hardly contributes to the measured surface in Fig. 3.

The cryo-FIB cross-section of the non-dispersed cement paste (Fig. 6) documents that irregularly shaped hydration rims form around the clinker particles within the initial period during the first few minutes. Different from well dispersed cement pastes, only few submicron particles can be observed in the interstitial pore space. Thus, in systems without PCE, early hydrates are instantaneously precipitating onto clinker surfaces and form agglomerates of a few microns in diameter. Those agglomerates represent flocculated bridges between the larger clinker particles which lead to the formation of an interconnected particle network. This microstructural observation can be correlated with the relatively high yield stress of fresh cement pastes without PCE compared to a cement paste containing PCE. A similar microstructural phenomena has been described for cement pastes at later hydration times close to the setting, where small interstitial grains (so-called SIGs) of approximately 2 μm form rigid bridges between the larger clinker grains [32]. The formation of a flocculated particle network based on the SIGs is associated with the physical transition at the time of setting. The observed agglomerates in the non-dispersed cement paste may represent precursors for these SIGs. The addition of PCE prevents the formation of such agglomerates (Fig. 7). Therefore the gyration radii of the particles are much smaller, which reduces the particle flocculation and leads to a decreased viscosity.

5. Conclusion

High pressure freezing enables the preservation of internal 3D structures of fresh cement pastes. Combined with cryo-FIB sectioning and high resolution cryo-SEM, the cryo-method provides a powerful tool for microstructural investigations of original particle structures in fresh cement pastes. For the first time, spatial distribution of suspended cement particles and hydrates can be investigated time resolved. Nevertheless, the cryo-methods are very time consuming and the present study only represents preliminary observations.

Cryo-FIB cross-sectioning opens new possibilities for investigations on long range particle structures (networks), development of hydration rims, spatial distribution of hydrates (in our example mainly ettringites) and formation of agglomerates. Cryo-FIB cross-section covers a representative area, whereas high resolution cryo-SEM investigations are more suitable for detailed morphological investigation of very fine structures on specific locations such as interfaces or particle surfaces.

This advanced microscopy technique has been applied for investigations on the impact of PCE on the microstructural development of fresh cement pastes. The following hypotheses can be formulated from the preliminary study on high pressure frozen cement pastes after few minutes of hydration:

1. In absence of PCE, early hydrates (ettringites) tend to precipitate on clinker surfaces (hydration rims) and tend to form agglomerates (SIGs), which will lead to interlocking bridges and thus, to higher yield stresses at later hydration times (setting).
2. Hydration rims around clinker particles in cement pastes without PCE are relatively thick compared to those in cement pastes with PCE. In both cases, at early hydration times, the rims do not cover the particle surfaces homogeneously and their thickness is not constant.
3. The interstitial pore space in cement pastes without PCE is almost free of smallest hydrate particles. In contrast, in presence of PCE, the hydrates (mainly ettringites) are well dispersed in the interstitial pore space and only minor amounts are attached on the clinker surfaces. With PCE, almost no agglomerates are formed during the first minutes of hydration. Yield stress and viscosity of such cement pastes are lower than in cement pastes without PCE.
4. The addition of PCE influences the volume of hydration phases and their spatial distribution (Figs. 5 and 6). This effect leads to changes of the particle size distribution, specific surface area

and numbers of particle and thus, changes the rheological behaviour of fresh cement pastes.

The cryo techniques presented in this study open new possibilities for the investigation of the formation of hydrates, their spatial distribution, the development of particle agglomeration and the formation of long range particle networks. Further cryo-studies shall be performed with different cement–PCE-systems and for different hydration times. This information is needed for a more profound understanding of the rheological effects of PCE.

Acknowledgments

The authors would like to address their thanks especially to EMEZ (Center for Electron Microscopy at the Swiss Federal Institute of Technology, (ETH) Zurich). We also would like to thank BASF AG, Ludwigshafen (Germany) for the financial support of this study.

References

[1] H. Uchikawa, S. Hanehara, T. Shirasaka, D. Sawaki, Effect of admixture on hydration of cement, adsorptive behavior of admixture and fluidity and setting of fresh cement paste, Cement and Concrete Research 22 (6) (1992) 1115–1129.
[2] H. Uchikawa, S. Hanehara, D. Sawaki, The role of steric repulsive force in the dispersion of cement particles in fresh paste prepared with organic admixture, Cement and Concrete Research 27 (1) (1997) 37–50.
[3] S. Hanehara, K. Yamada, Interaction between cement and chemical admixture from the point of cement hydration, adsorption behaviour of admixture, and paste rheology, Cement and Concrete Research 29 (8) (1999) 1159–1165.
[4] R.J. Flatt, Y.F. Houst, A simplified view on chemical effects perturbing the action of superplasticizers, Cement and Concrete Research 31 (8) (2001) 1169–1176.
[5] K. Yamada, T. Takahashi, S. Hanehara, M. Matsuhisa, Effects of the chemical structure on the properties of polycarboxylate-type superplasticizer, Cement and Concrete Research 30 (2) (2000) 197–207.
[6] E. Sakai, K. Yamada, A. Ohta, Molecular structure and dispersin-adsorption mechanisms of comb-type superplasticizers used in Japan, Journal of Advanced Concrete Technology 1 (1) (2003) 16–25.
[7] F. Winnefeld, S. Becker, J. Pakusch, T. Götz, J. Kaufmann, Struktur-Wirkungsbeziehungen von Polycarboxylatether - Fliessmitteln, Tagung Bauchemie, Monographie Bd., 35, GDCh-Fachgruppe Bauchemie, Berlin, 2005, pp. 330–335.
[8] F. Winnefeld, S. Becker, J. Pakusch, T. Gotz, Effects of the molecular architecture of comb-shaped superplasticizers on their performance in cementitious systems, Cement and Concrete Composites 29 (4) (2007) 251–262.
[9] B. Moeser, REM- und EDX-Untersuchungen an Betonen, Wiss. Z., 42, Bauhaus-Universitaet Weimar, 1996, pp. 61–74.
[10] K.O. Kjellsen, B. Lagerblad, H.M. Jennings, Hollow-shell formation — an important mode in the hydration of Portland cement, Journal of Materials Science 32 (11) (1997) 2921–2927.
[11] F. Kreppelt, M. Weibel, D. Zampini, M. Romer, Influence of solution chemistry on the hydration of polished clinker surfaces — a study of different types of polycarboxylic acid-based admixtures, Cement and Concrete Research 32 (2) (2002) 187–198.
[12] K.O. Kjellsen, A. Monsoy, K. Isachsen, R.J. Detwiler, Preparation of flat-polished specimens for SEM-backscattered electron imaging and X-ray microanalysis — importance of epoxy impregnation, Cement and Concrete Research 33 (4) (2003) 611–616.
[13] C. Rössler, J. Stark. Der Einfluss von Fliessmitteln auf die Hydratation von Portlandzement. in 15. Ibausil. Weimar 2003. 2: p. 508-522.
[14] S. Diamond, The microstructure of cement paste and concrete — a visual primer, Cement and Concrete Composites 26 (8) (2004) 919–933.
[15] K.L. Scrivener, Backscattered electron imaging of cementitious microstructures: understanding and quantification, Cement and Concrete Composites 26 (8) (2004) 935–945.
[16] C.C. Donaldson, J. McMahon, R.F. Steward, D. Sutton, The characterisation of structure in suspensions, Colloids and Surfaces 18 (2-4) (1986) 373–393.
[17] H.M. Wyss, M. Hütter, M. Müller, L.P. Meier, L.J. Gauckler, Quantification of microstructures in stable and gelated suspensions from cryo-SEM, Journal of Colloid and Interface Science 248 (2) (2002) 340–346.
[18] H.M. Wyss, E. Tervoort, L.P. Meier, M. Müller, L.J. Gauckler, Relation between microstructure and mechanical behavior of concentrated silica gels, Journal of Colloid and Interface Science 273 (2) (2004) 455–462.
[19] S. Metha, R. Jones, B. Caveny, Cryogenics with cement microscopy redefines cement behavior, Oil & Gas Journal 10 (1994) 47–53.
[20] H. Poellmann, J. Goeske, H.G. Pankau, Application of cryo-transfer scanning electron microscopy for investigation of cement hydration and cementitious systems, Twenty-Second International Conference on Cement Microscopy, 1, International cement microscopy association, Montreal, Quebec, Canada, 2000, pp. 310–331.
[21] J. Goeske, H. Poellmann, H.G. Pankau, Hydration of high alumina cement investigations with low temperature SEM (cryo-technique), Calcium Aluminate Cements, 1, University Press Cambridge, Heriot-Watt University Edinburgh, Scotland, UK, 2001, pp. 189–196.
[22] M. Fylak, J. Goeske, W. Kachler, R. Wenda, H. Poellmann, Cryotransfer scanning electron microscopy for the study of cementitious systems, European Microscopy and Analysis 20 (4) (2006) 9–12.
[23] U. Riehle. Über die Vitrifizierung verdünnter wässriger Lösungen. ETH (Swiss Federal Institute of Technology) Zurich, PhD-Thesis, 1968.
[24] R. Menold, B. Lüttge, W. Kaiser, Freeze-fracturing, a new method for the investigation of dispersions by electron microscopy, Advances in Colloid and Interface Science 5 (4) (1976) 281–335.
[25] L. Bachmann, E. Mayer, Physics of water and ice: implications for cryofixation, in: R.A. Steinbrecht, K. Zierold (Eds.), Cryotechniques in Biological Electron Microscopy, Springer-Verlag, 1987, pp. 3–34.
[26] H. Moor, Theory and practice of high pressure freezing, in: R.A. Steinbrecht, K. Zierold (Eds.), Cryotechniques in Biological Electron Microscopy, Springer-Verlag, Berlin Heidelberg, 1987, pp. 175–191.
[27] L. Holzer, B. Muench, M. Wegmann, P. Gasser, FIB-nanotomography of particulate systems — Part I: particle shape and topology of interfaces, Journal of the American Ceramic Society 89 (8) (2006) 2577–2585.
[28] B. Muench, P. Gasser, L. Holzer, R.J. Flatt, FIB-nanotomography of particulate systems — Part II: particle recognition and effect of boundary truncation, Journal of the American Ceramic Society 89 (8) (2006) 2586–2595.
[29] L. Holzer, P. Gasser, A. Kaech, M. Wegmann, A. Zingg, R. Wepf, B. Muench, Cryo-FIB-nanotomography for quantitative analysis of particle structures in cement suspensions, Journal of Microscopy 227 (3) (2007) 216–228.
[30] T. Richter, C. Peuckert, M. Sattler, K. Koenig, I. Riemann, U. Hintze, K.-P. Wittern, R. Wiesendanger, R. Wepf, Dead but highly dynamic — the stratum corneum is divided into three hydration zones, Skin Pharmacology and Physiology 17 (5) (2004) 246–257.
[31] M. Ritter, D. Henry, S. Wieser, S. Pfeiffer, R. Wepf, A versatile high-vacuum cryo-transfer for cryo-FESEM, cryo-SPM and other imaging techniques, Microscopy and Microanalysis 5 (2) (1999) 424–427.
[32] L. Holzer, F. Winnefeld, B. Lothenbach, D. Zampini, The early cement hydration: a multi-method approach, 11th International Congress on the Chemistry of Cement ICCC. Durban, South-Africa, 2003, pp. 236–248.